International Journal of
Molecular Sciences

MDPI

Article

Micro-Computed Tomography Detection of Gold Nanoparticle-Labelled Mesenchymal Stem Cells in the Rat Subretinal Layer

Pooi Ling Mok [1,2,*], Sue Ngein Leow [3], Avin Ee-Hwan Koh [1], Hairul Harun Mohd Nizam [4], Suet Lee Shirley Ding [1], Chi Luu [5,6], Raduan Ruhaslizan [4], Hon Seng Wong [4], Wan Haslina Wan Abdul Halim [4], Min Hwei Ng [7], Ruszymah Binti Hj. Idrus [8], Shiplu Roy Chowdhury [7], Catherine Mae-Lynn Bastion [4], Suresh Kumar Subbiah [2,9], Akon Higuchi [10,11,12], Abdullah A. Alarfaj [12] and Kong Yong Then [4,*]

1 Department of Biomedical Science, Faculty of Medicine and Health Sciences, Universiti Putra Malaysia, 43400 UPM Serdang, Selangor, Malaysia; avin.keh@gmail.com (A.E.-H.K.); suetlee.ding@gmail.com (S.L.S.D.)
2 Genetics and Regenerative Medicine Research Center, Universiti Putra Malaysia, 43400 UPM Serdang, Selangor, Malaysia; sureshkudsc@gmail.com
3 Department of Ophthalmology, Hospital Sultanah Aminah, 80100 Johor Bahru, Johor, Malaysia; sue_ngein@yahoo.com
4 Department of Ophthalmology, Faculty of Medicine, UKM Medical Center, 56000 Cheras, Kuala Lumpur, Malaysia; hairulnizam@ppukm.ukm.edu.my (H.H.M.N.); ruhaslizan89@gmail.com (R.R.); whs1975@gmail.com (H.S.W.); afifiyad@yahoo.co.uk (W.H.W.A.H.); maelynnbdr@gmail.com (C.M.-L.B.)
5 Centre for Eye Research Australia, Royal Victorian Eye & Ear Hospital, Melbourne 3002, Australia; cluu@unimelb.edu.au
6 Department of Surgery (Ophthalmology), The University of Melbourne, Melbourne 3002, Australia
7 Tissue Engineering Centre, Universiti Kebangsaan Malaysia Medical Center, 56000 Cheras, Kuala Lumpur, Malaysia; angelaster3@gmail.com, (M.H.N.); shipluchy_56@yahoo.com (S.R.C.)
8 Department of Physiology, Universiti Kebangsaan Malaysia Medical Center, 56000 Cheras, Kuala Lumpur, Malaysia; ruszyidrus@gmail.com
9 Department of Medical Microbiology and Parasitology, Universiti Putra Malaysia, 43400 UPM Serdang, Selangor, Malaysia
10 Department of Chemical and Materials Engineering, National Central University, Jhong-li, Taoyuan 32001, Taiwan; akon.higuchi@gmail.com
11 Department of Reproduction, National Research Institute for Child Health and Development, Tokyo 157-8535, Japan
12 Department of Botany and Microbiology, King Saud University, Riyadh 11451, Saudi Arabia; aalarfajj@ksu.edu.sa
* Correspondence: rachelmok2005@gmail.com (P.L.M.); kythen@hotmail.com (K.Y.T.); Tel.: +60-13-986-8287 (P.L.M.); +60-17-6100-828 (K.Y.T.)

Academic Editors: Adriano Piatelli and Barbara Zavan
Received: 11 November 2016; Accepted: 21 December 2016; Published: 8 February 2017

Abstract: Mesenchymal stem cells are widely used in many pre-clinical and clinical settings. Despite advances in molecular technology; the migration and homing activities of these cells in in vivo systems are not well understood. Labelling mesenchymal stem cells with gold nanoparticles has no cytotoxic effect and may offer suitable indications for stem cell tracking. Here, we report a simple protocol to label mesenchymal stem cells using 80 nm gold nanoparticles. Once the cells and particles were incubated together for 24 h, the labelled products were injected into the rat subretinal layer. Micro-computed tomography was then conducted on the 15th and 30th day post-injection to track the movement of these cells, as visualized by an area of hyperdensity from the coronal section images of the rat head. In addition, we confirmed the cellular uptake of the gold nanoparticles by the mesenchymal stem cells using transmission electron microscopy. As opposed to other methods, the current protocol provides a simple, less labour-intensive and more efficient labelling mechanism for

real-time cell tracking. Finally, we discuss the potential manipulations of gold nanoparticles in stem cells for cell replacement and cancer therapy in ocular disorders or diseases.

Keywords: mesenchymal stem cells; gold nanoparticles; stem cell tracking; rat subretinal layer; transmission electron microscopy; micro-computed tomography

1. Introduction

Regenerative medicine is a fast-growing medical field that encompasses a wide array of techniques to replace and repair damaged tissues within the human body. Mesenchymal stem cells (MSCs), a type of adult stem cell, are widely studied owing to their potential in cellular-based regenerative therapies for treating a variety of medical conditions, including autoimmune [1], cardiovascular [2], and neurodegenerative [3] diseases. These stem cells are also utilized in the repair of bones and cartilage [4]. More recently, there has been growing interest in the use of MSCs to treat retinal diseases [5], partly due to their ability to differentiate into neurons [6]. In addition to being able to differentiate into different cell types [7], MSCs exert reparative effects by migrating to damaged tissues [8,9]. This cellular migration can be monitored for various scientific purposes with the use of histological techniques; however, the process is invasive, time-consuming, and does not allow for real-time tracking [10]. Thus, a more suitable method is required for investigating MSCs in vivo.

Nanoparticles are widely used to facilitate the study of the biodistribution, homing, and cell fate of transplanted cells in living animal models [11]. Gold nanoparticles (GNPs) are one such example, which can be modified to possess different sizes, shapes, and conjugated molecules that ultimately change the physical characteristics of the particles to suit different research needs [12,13]. The GNPs have been demonstrated to not affect the proliferation or cellular functions of MSCs, making them a viable option for in vivo cell tracking [14–16]. Moreover, no acute cellular toxicity was associated with the use of GNPs in human cells [17]. To date, GNPs have been widely used in a variety of research applications with MSCs, including as a contrast agent for cell tracking [18] as well as in differentiation studies [19,20] and anti-cancer research via photothermal therapy with cell-based vectors [21]. Thus, GNPs are attractive tools in MSC research. As such, we here report a simple protocol for the labelling of human Wharton's jelly-derived MSCs (hWJ-MSCs) with GNPs, as well as their detection following subretinal injection in the Royal College of Surgeon (RCS) rat model based on micro-computed tomography (micro-CT) and verification by electron microscopy.

2. Results

2.1. Characteristics of MSCs

The hWJ-MSCs exhibited a typical fibroblast-like morphology (Figure 1), and could differentiate into cells of the adipogenic and osteogenic lineages, which were visualized by Oil Red O and Alizarin Red S staining, respectively (Figure 2). Apart from this multipotent feature, flow cytometric analysis of the culture-expanded cells displayed a clear immunophenotypic characteristic (Figure 3). Specifically, the hWJ-MSCs expressed CD73 (94.6%), CD90 (100%), and CD105 (99.6%), but did not express CD14 (0.1%), CD34 (0%), CD45 (0.1%), CD80 (0%), and CD86 (12.2%). Taken together, these results confirmed that the cells were indeed MSCs, and the culture was not contaminated by any hematopoietic cells.

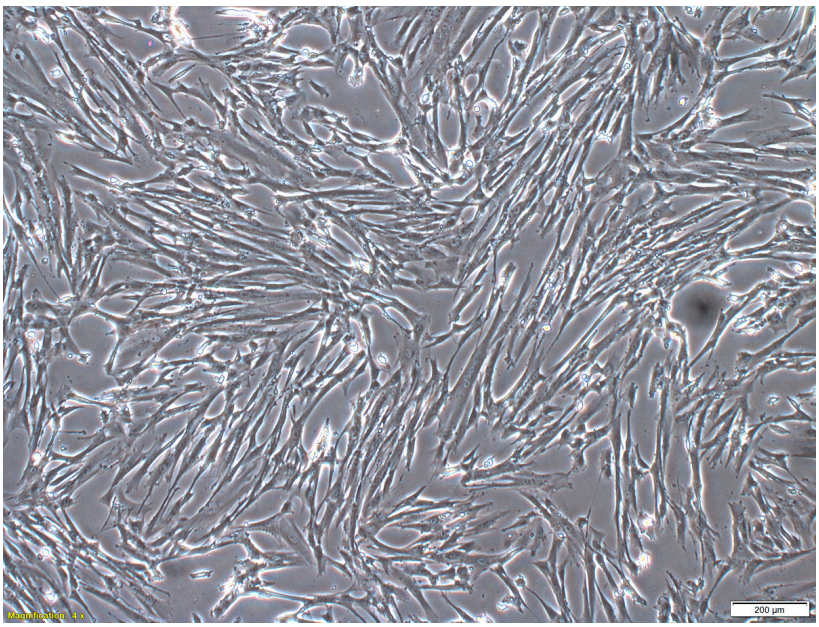

Figure 1. Morphology of human Wharton's jelly-derived mesenchymal stem cells (hWJ-MSCs). The culture-expanded cells (passage 3) were viewed under a phase-contrast microscope at a total magnification of 40×. The cells showed a fibroblast-like phenotype. The scale bar denotes 200 µm.

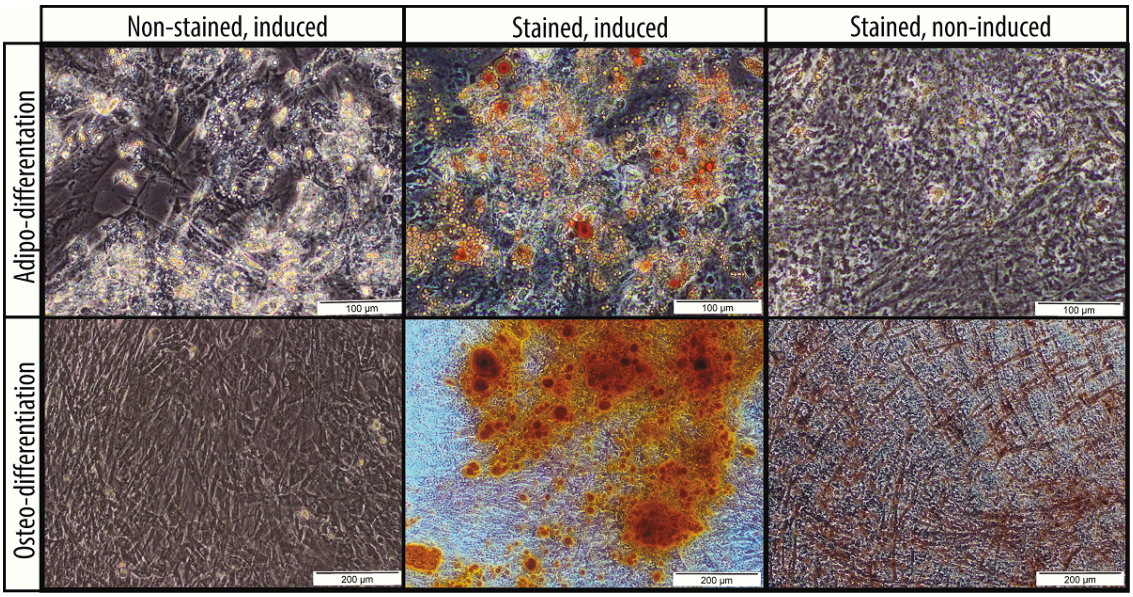

Figure 2. Adipo- and osteo-differentiation of human Wharton's jelly-derived mesenchymal stem cells (hWJ-MSCs). The presence of adipocytes was visualized by Oil Red O staining after the cells were induced for adipogenic differentiation as compared to the non-induced hWJ-MSCs (200× total magnification). The scale bars denote 100 µm. The presence of osteocytes was visualized by Alizarin Red S staining after the cells were induced for osteogenic differentiation as compared to the non-induced hWJ-MSCs (100× total magnification). The scale bars denote 200 µm.

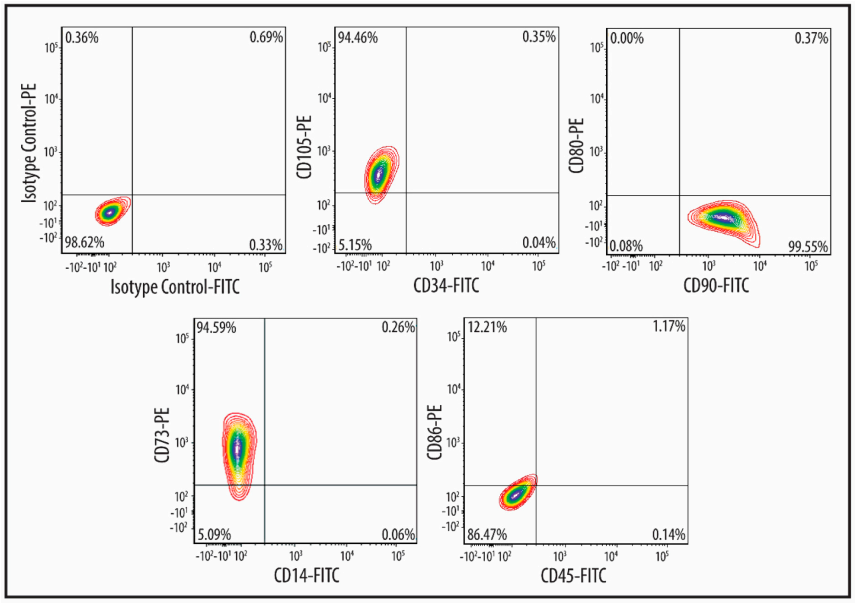

Figure 3. Immunophenotypic analysis of human Wharton's jelly-derived mesenchymal stem cells (hWJ-MSCs) using the FACSAria III system. The cells showed positive expression of CD105, CD90, and CD73, but not of CD34, CD45, CD14, CD80, and CD86.

2.2. Quality of GNPs

The colloidal GNPs were observed under a scanning electron microscope (SEM) to determine the size and shape of the particles. The colloid consisted of homogenous spherical nanoparticles with a size of approximately 80 nm (Figure 4). This step ensured that the particles were in good functioning condition for the subsequent experiment. The absorbance measurement of the particles had a single narrow absorbance peak at 545 nm [5].

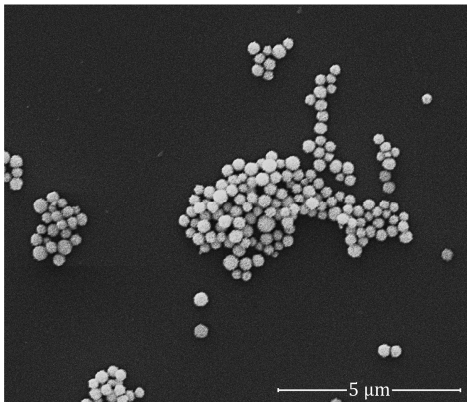

Figure 4. An image of the colloidal GNPs produced by a scanning electron microscope at 20,000× magnification. The particles showed spherical shapes of approximately 80 nm in diameter. The scale bar denotes 5 µm.

2.3. Cellular Uptake of GNPs by MSCs

The cells were incubated with 1.4×10^8 GNPs/mL in a six-well plate for 24 h. The supernatants were discarded and the cells washed with sterile phosphate-buffered saline (PBS) before phase-contrast microscopic images of the GNP-labelled cells were taken. As shown in Figure 5b, the presence of black particles was detected in the cytoplasm of the GNP-labelled hWJ-MSCs, whereas no black particles could be observed in the control cells (Figure 5a) cultured with sterile deionized water

only. Before injection into the subretinal layer of the rats, the cells were resuspended in sterile Hanks' balanced salt solution (HBSS). The pelleted cells were also assessed for the uptake of GNPs using transmission electron microscopy (TEM). As shown in Figure 6, a large number of enveloped (small vesicles, endosomes, etc.) black particles were detected within the cytoplasm of the MSCs.

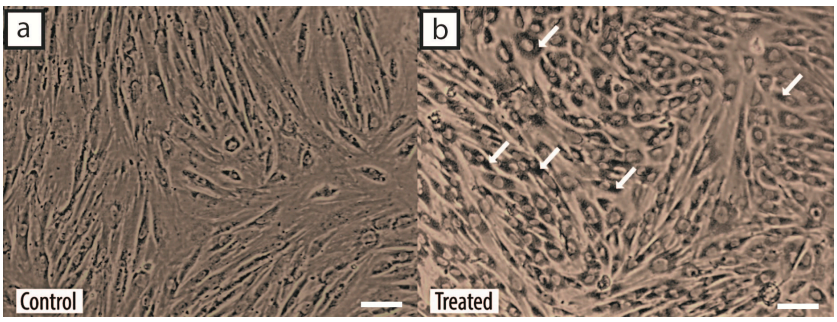

Figure 5. Cellular uptake of gold nanoparticles (GNPs). (**a**) Phase-contrast microscopic image of unlabelled human Wharton's jelly-derived mesenchymal stem cells (hWJ-MSCs). The scale bar denotes 100 μm; (**b**) phase-contrast microscopic image of GNP-labelled hWJ-MSCs, following 24 h of incubation with 1.4×10^8 GNPs/mL. The white arrows mark the presence of GNPs in the cytoplasm. The scale bar denotes 100 μm.

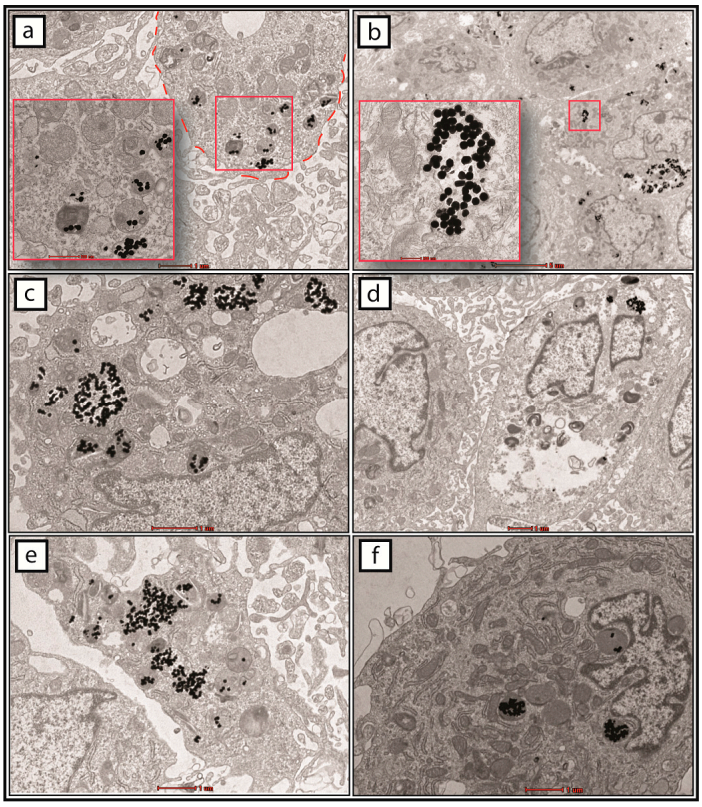

Figure 6. Imaging of gold nanoparticles (GNPs) in the human Wharton's jelly-derived mesenchymal stem cells (hWJ-MSCs) by transmission electron microscopy (TEM). The treated cells were harvested, pelleted, and processed after incubation with GNPs for TEM observations. (**a**–**f**) Spherical black particles were found to be internalized in small vesicles such as the endosomes. The red dash lines in (**a**) demarcates the boundary of a single cell. The scale bars denote 1 μm (**a**,**c**–**f**) and 5 μm (**b**). The scale bars denote 500 and 200 nm in inset images of (**a**,**b**), respectively.

2.4. Tracking of GNP-Labelled MSCs by Micro-CT

After the cells were incubated with GNPs and injected into the subretinal layer of the rats, they were tracked by micro-CT. The site of injection showed an area of hyperdensity, which remained detectable even at days 15 and 30 (Figure 7). With the aid of bright-field microscopy at the area of interest, the presence of black particles could be observed in the retina and choroidal tissue (Figure 8). After enucleating the eye, the localization of GNP-loaded cells was confirmed in the subretinal layer on day 30 using a transmission electron microscope, and was most notably detected in the retinal pigment epithelium (Figure 9).

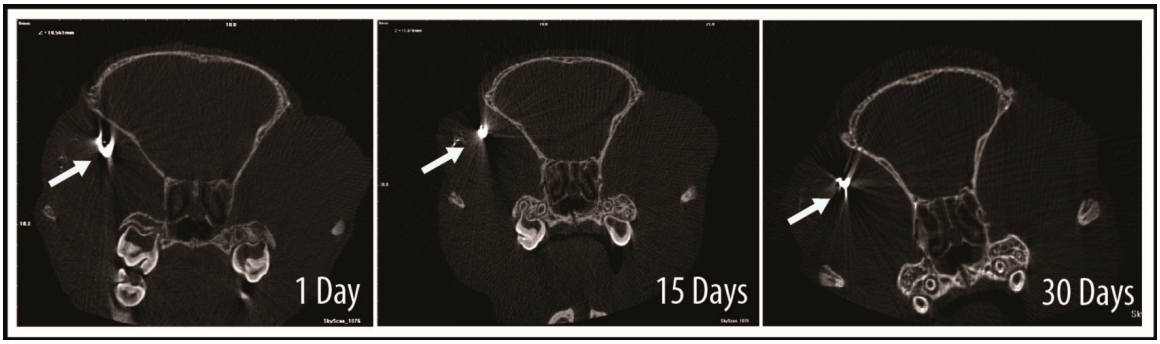

Figure 7. In vivo tracking of cells labelled with gold nanoparticles (GNPs) using micro-computed tomography (micro-CT). Micro-CT scanning showed hyperdensity in the superotemporal section 24 h after injection, as indicated by the white arrow. The hyperdensity remained detectable even after days 15 and 30.

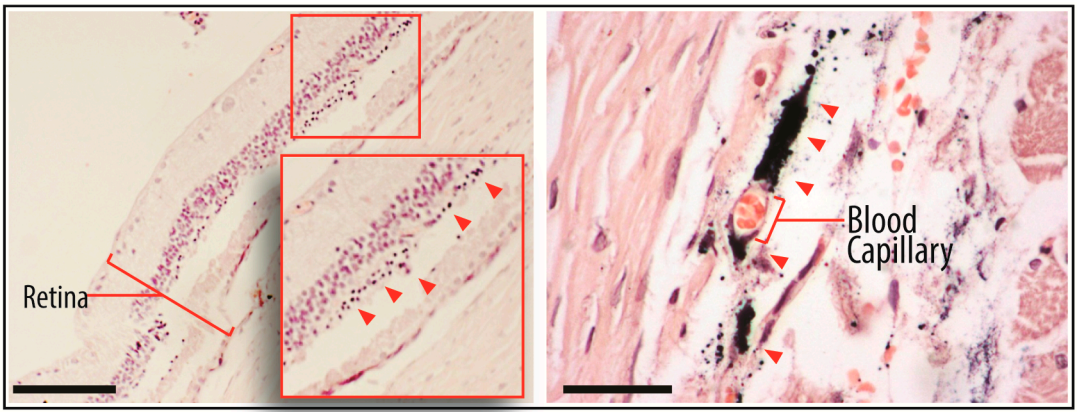

Figure 8. The eyes were harvested and processed for TEM imaging. The sections were stained with Toluidine Blue to localize the target tissue viewing area. (**Left**) Black particles were present in the subretinal layer, as observed under a bright-field imaging microscopy system at a total magnification of 40×, and indicated by the red arrows; (**right**) some particles were also found near the choroidal capillary of a tissue section at a total magnification of 400×.

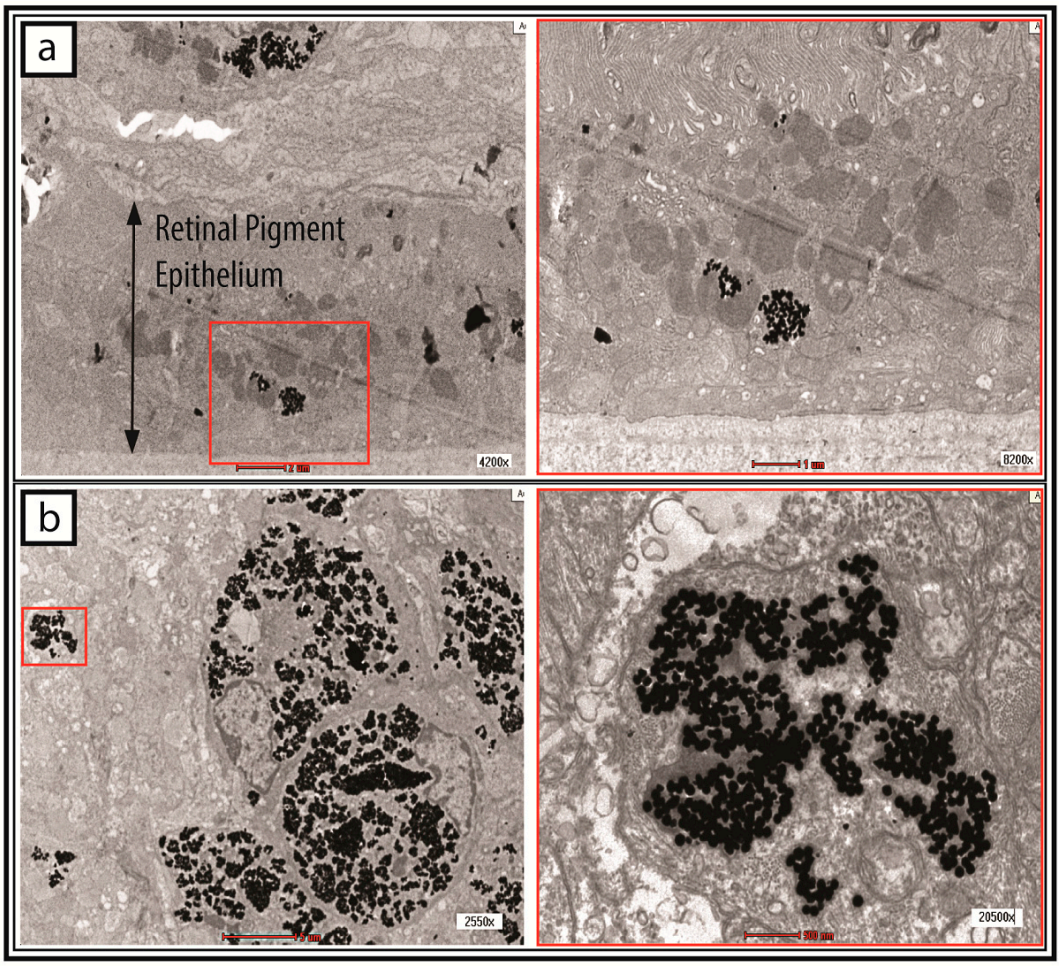

Figure 9. Detection of gold nanoparticle (GNP)-labelled cells in the subretinal layer of the eye by transmission electron microscopy (TEM). (**a**) GNP-labelled cells were found to be present in the retinal pigmented epithelium; the scale bar denotes 2 μm (**left**) and 1 μm (**right**); (**b**) The cells containing the black particles incorporated themselves within the host tissue; the scale bar denotes 5 μm (**left**) and 500 nm (**right**).

3. Discussion

In this study, we labelled MSCs with GNPs for the purpose of in vivo cell tracking in RCS rats. The MSCs were successfully culture-expanded from human Wharton's jelly (hWJ-MSCs) (Figure 1) and were shown to be multipotent, since the cells were able to differentiate into adipocytes and osteocytes, which are both part of the mesoderm lineage (Figure 2). These cells highly expressed CD73, CD90, and CD105, but lacked expression of CD14, CD34, and CD45 (Figure 3), indicating the absence of contaminating hematopoietic cells in the culture [22]. In accordance with previous reports, these cells also demonstrated a lack of the co-stimulatory molecules CD80 and CD86 [23], conferring the ability to escape from immune surveillance. The immunophenotypic characteristics of the cultured cells satisfied the criteria for MSC surface markers as defined by the International Society for Cellular Therapy [24].

MSCs hold immense promise in cellular-based regenerative therapies, but the mechanisms by which these cells repair damaged tissues are complex, and invasive methods are often required for analysis, which may result in the premature death of in vivo models [25]. As such, the ability to track these cells with GNPs in real time before animal sacrifice offers more advantages to researchers, such as observing cellular migration patterns and assessing the effectiveness of cell therapy [26]. Prior to labelling the hWJ-MSCs with GNPs, our assessment on the integrity of the particles showed no signs of dysfunction; the aggregates of GNPs were consistently spherical in shape and were around

80 nm in size (Figure 4). In addition, the particles did not exhibit any shift in absorbance at its optimal wavelength of 545 nm. Following treatment with GNPs, the presence of black spots was observed in the cytoplasm of the cells under a phase-contrast microscope (Figure 5). These spots were the GNPs that were taken up via receptor-mediated endocytosis and retained within the endosomes, which would then fuse with lysosomes for processing before being excreted by the cells [27,28]. We confirmed the presence of the particles by TEM observations of the cells collected following incubation with GNPs (Figure 6a–f). Indeed, the cells contained dark vesicle-bound GNPs that were highly suggestive of endosomes. Evaluation of the supernatants collected from the co-incubation of MSCs and GNPs indicated a null value of absorbance at 545 nm, which demonstrated that all the particles had been taken up by the MSCs.

With the accumulation of GNPs in hWJ-MSCs, the cells could be much more easily tracked and distinguished from the surrounding endogenous tissue in the rat using micro-CT and TEM. The micro-CT image (Figure 7) showed an area of hyperdensity following subretinal post-injection in one eye, and the signal remained detectable even after 30 days. In addition, we observed the presence of GNPs around the choroidal capillary in a tissue section stained by Toluidine Blue (Figure 8). One limitation involving nanoparticle labelling is the non-specific uptake of particles by the mononuclear phagocytic/reticuloendothelial system upon the death of the labelled cells [29]. As is the case for the injection of any cell type into an inflamed tissue site, not all cells can survive in the harsh microenvironment. As such, the injected cells would be ultimately phagocytosed by the surrounding immune cells and transported for clearance via the blood circulation. Indeed, the hepatic clearance of GNPs has been observed [30]. In spite of this potential limitation, the TEM histological images (Figure 9) strongly confirmed the presence of GNP-labelled cells in the subretinal layer of the rat, particularly in the retinal pigment epithelium (RPE). Several studies [31–33] have demonstrated that MSCs are capable of differentiating into the RPE. Therefore, the presence of GNPs in the RPE could indicate that the transplanted hWJ-MSCs were incorporated into the host RPE to facilitate cellular repair. It is also possible that the phagocytic nature of the RPE resulted in the uptake of GNPs from phagocytosed hWJ-MSCs, since these cells play a role in the phagocytic maintenance and renewal of photoreceptor outer segments [34,35]. Further studies (e.g., immunohistochemistry) are needed to distinguish between these two possibilities. Overall, the results of this study demonstrated the robustness of our protocol, especially in regards to the long-term presence of GNPs, which were retained 30 days after the transplantation procedure.

Various types of cell trackers have been designed to determine the cell fate in an in vivo system. The choice of cell trackers largely depends on the ease of preparation, cost, and capability of the imaging system, and whether or not it will disturb cellular viability and function. Table 1 describes the cell labelling technologies that are commonly used in pre-clinical research. Several methods have been developed for labelling MSCs. Indirect cell labelling involves the overexpression of reporter genes such as the ferritin (Fth1) [36] and transferrin receptor (TfR1) genes [37] before the cells are imaged by magnetic resonance imaging (MRI). In contrast, MSCs can also be directly labelled with nanoparticles such as GNPs. Other examples include superparamagnetic iron oxide nanoparticles and quantum dots, in which the former is detectable by MRI [38], while the latter is a fluorescence-based technique [39].

Compared to other methods, GNPs are relatively cost-effective and simple to utilize in cell labelling. Only a few reports have been published on the effects of GNP uptake for the cellular viability and function of MSCs. It has been suggested that the size and shapes of nanoparticles could affect the viability and differentiation potential of MSCs. For instance, Fan et al. [40] found that the size of a GNP affected its cellular toxicity and proliferation, i.e., GNPs of smaller sizes caused higher cytotoxicity and reduced the formation of colony-forming unit-fibroblasts by human bone marrow-derived MSCs, and vice versa. Furthermore, Li et al. [16] reported that GNPs could influence osteogenic differentiation by regulating the activation of Yes-associated protein. We have reported the cell viability with LIVE/DEAD staining and proliferation using CellTiter-Glo reagent upon successful

labelling with 80 nm of GNPs. Both cell viability and proliferation were not significantly affected by the uptake of GNPs even after 10 days of continuous cell culture [5].

Our current study provides evidence for the successful labelling of hWJ-MSCs with GNPs, and the localization of the labelled cells in the subretinal layer of an RCS rat model. In our previous study [5], we suggested the possible differentiation of unlabelled MSCs into rod photoreceptors, bipolar, and Müller glial cells using the same rat model. Hence, future studies should evaluate the possible effects of GNP for directing the differentiation of MSCs into retinal neuron cells and the underlying mechanisms. This might lead to new knowledge and methods to treat blindness caused by retinal degenerative disorders [41]. Wang et al. [42] reported that a low concentration of gold/Fe_3O_4 promoted the differentiation of rat olfactory bulb stem cells into neural precursor cells. Paviolo et al. [43] demonstrated that poly(4-styrenesulfonic acid)-coated and SiO_2-coated gold nanorods could be taken up by NG108-15 neuronal cells (a neural cell line of neuroblastoma × glioma hybrid). Upon exposure to laser light at the plasmon resonance wavelength, the gold nanorods could induce the differentiation process in nanoparticle-treated cells, as indicated by increases in the neurite length, number of neurites per neuron, and the percentage of neurons with neurites.

The GNP-labelled cells may also offer a new form of treatment for eye cancers such as retinoblastoma and choroidal melanoma, since MSCs possess the ability to migrate to tumour cells [21]. Large GNPs (80 nm) can absorb light and convert it into heat energy [44], leading to cancer cellular destruction. On the other hand, the destruction of MSCs can result in the release of cytokines and trophic factors, which would further aid in tissue repair and regeneration [45]. Specifically, MSCs secrete brain-derived neurotrophic factor, basic fibroblast growth factor, and ciliary neurotrophic factor, which could help in retinal neuron cell regeneration [14]. A clinical trial [46] was initiated in 2011 on the application plasmonic photothermal and GNP technology in stem cells to destroy atherosclerotic plaques. Unfortunately, the trial was terminated due to unknown circumstances. In the case of eye cancer, GNP-loaded cells could be modified at the surface membrane [47,48] to improve the targeting and killing of eye cancer.

Table 1. Cell labelling technologies used in preclinical studies.

Cell Labelling Technology	Advantages/Disadvantages	References
Viral or non-viral reporter gene systems	Advantages: Allows monitoring of co-expressed genes.	[49]
	Disadvantages: Labour-intensive and time-consuming in the preparation of transduced cell clones. Radioactive substance is required in a conventional chloramphenicol acetyl transferase reporter system, which is potentially hazardous.	[16,50]
Free organic dyes e.g., PKH26, carboxyfluorescein succinimidyl ester (CFSE)	Advantages: Simple cell-labelling protocol. Long-term cell tracking in both in vitro and in vivo systems, e.g., PKH26.	[51]
	Disadvantages: Possible transfer of dye from labelled to unlabelled cells.	[52]
Organic dye nanoparticles	Advantages: Suitable for living-cell imaging as it demonstrates high fluorescence intensity, large Stokes shift, photostability, and emission in the near-infrared range.	[53]
	Disadvantages: High tendency of organic dye to stick to the cell substrate.	[54]
Superparamagnetic iron oxide nanoparticles (SPIO)	Advantages: Direct tissue targeting of SPIO-labelled cells is feasible with use of an appropriate magnetic field.	[55]
	Disadvantages: Requires cross-linking with a membrane-translocating signal peptide (e.g., HIV-1 Tat protein) or co-incubation with transfection agents to facilitate cellular uptake.	[25]
Semiconductor quantum dots	Advantages: Photostable, possesses size-controlled fluorescence, and the emitted fluorescence has a long lifetime.	[56]
	Disadvantages: High cost of reagents; generation of free radicals may cause cellular toxicity.	[57,58]
Noble metallic nanoparticles e.g., gold nanoparticles	Advantages: Simple cell-labelling protocol and no acute cellular toxicity demonstrated.	[59]
	Disadvantages: Different shapes and sizes could affect stem cell differentiation potential.	[16,40]

4. Materials and Methods

4.1. MSC Culture Conditions

The culture of MSCs (hWJ-MSCs) was obtained from a local stem cell bank (Cryocord, Cyberjaya, Selangor, Malaysia) and provided in the form of cryovials. The source of the tissue was the umbilical cord-isolated Wharton's jelly of a woman at full-term gestation, who provided informed consent.

The cell number and viability in the cryovials were determined by performing a Trypan Blue exclusion test. Cells in 1 mL of the cryopreservative were transferred into a 10-mL centrifuge tube containing 9 mL of sterile PBS at room temperature (RT) of 25 °C. The tube was then centrifuged at 200× *g* for 10 min. Following centrifugation, the cells were resuspended in 1 mL of hWJ-MSCs culture medium. The cell concentration and viability were determined using 0.4% Trypan Blue reagent.

The hWJ-MSCs were seeded at a density of 5×10^3 cells/cm^3 into a T-75 culture flask in 10 mL of culture medium. The culture medium was prepared by supplementing Dulbecco's modified Eagle's medium (DMEM)-low glucose with 10% (*v*/*v*) foetal bovine serum (FBS) (Thermo Fisher Scientific, Waltham, MA, USA), 100 U/mL penicillin, 100 µg/mL streptomycin, and 0.25 µg/mL amphotericin b (Thermo Fisher Scientific, Waltham, MA, USA). The culture flasks were immediately stored at 37 °C in an incubator supplemented with 5% CO_2. The culture medium was changed every three days. The supernatant was aspirated before the addition of 10 mL of fresh culture medium each time, and the cultures were incubated at 37 °C, 5% CO_2.

Subculture was performed when the cells reached 80%–90% confluence. The supernatant was aspirated before washing and rinsing two times with 5 mL of sterile PBS. The cells were then incubated with 5 mL of 0.25% trypsin/ethylenediaminetetraacetic acid (EDTA; Thermo Fisher Scientific) for 5 min in a CO_2 incubator at 37 °C. Immediately upon observation of cell detachments, 5 mL of culture medium were added to inactivate the trypsin/EDTA at RT. The medium containing the cells was aspirated using a 10-mL pipette and transferred to a 50-mL centrifuge tube. The tube was then centrifuged at 200× *g* for 10 min. Following centrifugation, the supernatant was discarded and the cell pellet was suspended again in 10 mL of PBS. The tube was then centrifuged at 200× *g* for 10 min. The cell concentration and viability were determined according to the Trypan Blue exclusion test as described above. The above culture protocol was repeated to expand the cells to obtain a sufficient cell number for the experiments. Cell cryopreservation was also carried out to preserve the cells for future studies. For cryopreservation, the cell pellet containing approximately 1×10^6 cells (obtained after centrifugation as indicated above) was suspended in 1 mL of cold cryopreservation medium containing 90% FBS and 10% dimethyl sulfoxide (Thermo Fisher Scientific), and transferred into a 1-mL cryovial. The cryovial was kept overnight at −80 °C in a cryocool box. The cryovial was transferred into a liquid nitrogen tank and stored in the vapour phase until future use.

4.2. MSC Characterization

Only cells at passage 3–8 were used for the experiments in this study. To assess the multipotency of the hWJ-MSCs, adipogenic (Cat no. SCR020) and osteogenic (Cat no. SCR028) differentiation assays were performed using kits according to the manufacturer instructions (Merck Millipore, Billerica, MA, USA). To confirm the presence of specific surface markers, the hWJ-MSCs were immunophenotyped by flow cytometry using a cocktail of anti-human CD105 (Cat no. FAB10971P, 5 µL), CD73 (Cat no. 550257, 5 µL), CD90 (Cat no. 555595, 2500 µg), CD34 (Cat no. 348053, 0.625 µg), CD45 (Cat no. 347463, 0.25 µg), CD14 (Cat no. 347493, 0.125 µg), CD80 (Cat no. 340294, 0.15 µg), and CD86 (Cat no. 555658, 5 µL) antibodies (each per 1×10^5 cells). All antibodies, except for CD105 (R&D Systems, Minneapolis, MN, USA), were obtained from BD Pharmingen (BD Biosciences, San Jose, CA, USA).

4.3. GNP Labelling: Determination of the Quality of Colloidal GNPs

The colloidal GNPs used in the current study were obtained from BBI (BBI Solutions, Madison, WI, USA). The size of these GNPs is 80 nm with a spherical shape. The sterile colloidal solution was kept under aseptic conditions at 4 °C at all times. To ensure the long-term stability and integrity of the colloidal GNPs, a spectrophotometer was used to determine the optimal absorption wavelength of the colloid.

To achieve this, the bottle containing the colloidal solution was gently inverted five times to homogenously suspend the GNPs. A volume of 1 mL was aspirated using a pipette tip at RT and transferred into cuvettes for spectrophotometry. The absorbance was determined across a wide wavelength range (200–700 nm). The optimal absorption wavelength of the GNPs in deionized water was also determined. One millilitre of the colloid was aspirated into a 1.5-mL Eppendorf tube and centrifuged at 6000× *g* for 10 min to pellet the GNPs. The pelleted GNPs were then added to 1 mL of deionized water and transferred into cuvettes for spectroscopic measurement as described above.

To confirm the physical size and shape of the GNPs, SEM was performed. A volume of 1 mL was aspirated using a pipette tip at RT and directly deposited onto a silicon chip for SEM. The particles were imaged using an FEI Helios Dual-Beam SEM-based measuring system (FEI Company, Hillsboro, OR, USA), which was equipped with a high-performance electron beam column and sample stage.

4.4. GNP Labelling: Cell Incubation with GNPs

Prior to the cell labelling experiment with GNPs, the hWJ-MSCs were cultured on a six-well plate at a seeding density of 5×10^3 cells/cm^3 in 2 mL of culture medium. The cells were incubated in a CO_2 incubator at 37 °C until reaching 70% confluence (approximately 12–16 h).The supernatant in the six-well plate was discarded and the cells were washed twice using 2 mL of sterile PBS at RT. The cells were then added to 1 mL of DMEM and incubated in a CO_2 incubator at 37 °C until the addition of GNPs.

The colloidal GNPs in the bottle were inverted five times at RT. One millilitre of the colloid was aspirated into a 1.5-mL Eppendorf tube. The tube was centrifuged at 6000× *g* for 10 min to pellet the GNPs. The supernatant was discarded following centrifugation, and the pelleted GNPs were then resuspended in 1 mL of DMEM to attain a final concentration of 1.4×10^8 particles/mL. The suspended GNPs were then added into each well (200 µL/cm^2) containing the prepared hWJ-MSCs. The cells were observed under a phase-contrast microscope before stored in a CO_2 incubator at 37 °C for 24 h.

After 24 h, the culture medium from the wells was harvested and collected in a 15-mL centrifuge tube to determine the remnant GNPs by measuring the absorbance value at 545 nm according to the protocol described in Section 4.3. The cell culture medium was replaced with fresh full culture medium containing 10% (*v*/*v*) FBS, 100 U/mL penicillin, 100 µg/mL streptomycin, and 0.25 µg/mL amphotericin. The six-well plate was then immediately placed in a CO_2 incubator at 37 °C until subretinal transplantation. For subretinal transplantation, the cells were trypsinized, and washed at least two times before resuspension in HBSS. The cells were immediately used for injection as described below in Section 4.6.

4.5. GNP Labeling: Determination of the Cellular Uptake of GNPs

To confirm that all GNPs were taken up by the hWJ-MSCs, the culture medium harvested from the cell incubation step (Section 4.4) was assessed for the presence of GNPs. The collected culture medium was first centrifuged at 6000× *g* for 10 min. The supernatant was then discarded, and 1 mL of deionized water was added. The added deionized water was gently flicked and then transferred into a cuvette for absorbance measurement according to the protocol outlined in Section 4.3.

The presence of GNPs taken up by the cells was visualized with TEM of the cytoplasm. The supernatant was aspirated before washing and rinsing two times with 2 mL of sterile PBS.

The cells were incubated with 0.5 mL of 0.25% trypsin/EDTA for 5 min in a CO_2 incubator at 37 °C. Immediately upon observation of cell detachments, 0.5 mL of the culture medium was added to inactivate the trypsin/EDTA at RT. The medium containing the cells was aspirated using a 1-mL pipette and transferred to a 50-mL centrifuge tube. The tube was then centrifuged at 200× *g* for 10 min. Following centrifugation, the supernatant was discarded and the cell pellet was suspended again in 2 mL of PBS. The tube was then centrifuged at 200× *g* for 10 min. The supernatant was discarded to collect the cell pellet for TEM imaging.

4.6. Subretinal Injection of GNP-Labelled MSCs

The study was approved by the Universiti Kebangsaan Malaysia Animal Ethics Committee (UKMAEC) (Approval no: PP/OPHTAL/2011/HASLINA/22-MARCH/363-APRIL-2011-DECEMBER-2012) on March 2011. The animal experiments were conducted according to the guidelines provided by UKMAEC and conformed to the ARVO Statement for the Use of Animals in Ophthalmic and Vision Research. All the instruments used were autoclaved before the cell injection procedure was conducted. The RCS rats used in this experiment were between 18 and 21 days old. The rats were first anesthetized by intraperitoneal injections of ketamine (80 mg/mL) and xylazine (12 mg/mL) (Sigma-Aldrich, St. Louis, MO, USA) based on a 100 µL/10 g body weight dosage. The hind paws were pinched to ensure that the rats were properly anaesthetized, and dilating eye drops were instilled in both eyes. After 5 min, or once adequate anaesthesia was achieved, the rats were positioned under a stereomicroscope on their abdomen with the eyes facing the microscope lens. The eyes and fundus of the rats were checked to ensure that no abnormalities were present. A traction suture was placed on the conjunctiva to expose the site of the intended injection, which was located temporosuperiorly. Conjunctival periotomy was performed to expose the bare sclera. A 30-G sharp needle was then carefully used to introduce a small hole behind the limbus at an oblique angle, and care was taken to not penetrate the needle into the lens. Then, 2×10^5 GNP-labelled MSCs in sterile HBSS solution were loaded into syringes equipped with a 30-G blunt needle.

The blunt needle was then carefully inserted through the same track, and the cells were slowly injected into the subretinal space. After injection, the syringe was carefully retracted, and the site of injection was marked with a nylon suture. The fundus was examined for a subretinal bulge, and eyes with complications such as inadvertent vitreous injection, vitreous haemorrhage, or retinal detachment were excluded. Finally, antibiotic ointment was applied to the eye and the rats were gently placed back in the recs inadvertent viovery chamber until they regained full consciousness.

4.7. Micro-CT of Treated Rats

At days 1, 15, and 30 post-injection, the rats injected with GNP-labelled hWJ-MSCs were anesthetized with similar doses described above and carefully fastened onto a CT bed. The bed position was adjusted to fit under the field of view of the scanner. Micro-CT was then conducted by an experienced operator, with a source spot size of 8.88 µm at 45 kVp (with 0.5-mm AI filtering). The rats were finally released from the harness and returned to their cages to be kept under monitoring from time to time.

4.8. TEM of Injected MSCs

To track the injected MSCs in the eyes, the rats were sacrificed at 30 days post-injection. The rats were first secured in a restrainer with their tails exposed. Euthanasia was performed using a drug overdose by intravenous injections of sodium pentobarbital (Sigma-Aldrich, St. Louis, MO, USA) into the rat tail vein at a dosage of 150 mg/kg. The skin around the eyes of the rats was stretched to allow the eye to slightly pop out. A pair of dissecting scissors was used to sever the optic nerve, allowing the eyeballs to be harvested. The harvested eye cups containing the injected MSCs were fixed by immersing the samples in sterile 0.1 M phosphate buffer (pH 7.4) with 2.5% glutaraldehyde solution for 1 h at RT. The samples were then washed with 0.2 M phosphate buffer, and the eye cups

were treated with 1% osmium tetroxide solution (OsO_4) in 0.1 M phosphate buffer for 1 h, and then washed at least five times in distilled water.

En bloc staining was performed in 2% aqueous uranyl citrate in the dark for 2 h at 4 °C. The samples were then dehydrated with graded ethanol (35% to 100%, with a 15-min dehydration period each) and treated with epoxy propane before embedding in 812 resin overnight. The embedding moulds were left to cure for 24 h at 60 °C, and then the embedded tissues were sectioned serially using a diamond knife on an ultramicrotome to first achieve a thickness of 500 nm. The sections were stained with 1% Toluidine Blue and viewed under a microscope to identify the site of interest in the retina. Subsequently, 76-nm tissue slices were collected on a slot grid, and then stained with uranyl acetate for 2 h and with lead citrate for 5 min.

Once the sections were washed, TEM images were taken by an experienced operator using a Tecnai G2 Spirit Biotwin system (FEI Company). The uptake of GNPs into the cytoplasm of hWJ-MSCs was assessed and confirmed using TEM following essentially the same protocol as described above. However, the cells were collected by first centrifuging at 400× *g* and washed with PBS twice before cell fixation.

5. Conclusions

In conclusion, we have provided a simple protocol for labelling human Wharton's jelly-derived Mesenchymal Stem Cells (MSCs) with GNPs for in vivo cell tracking. MSCs are suitable candidate for cell replacement therapy, particularly due to their easy isolation and expansion from adult tissues, differentiation potential, homing abilities to site of injury and immunomodulatory properties. Many studies have evinced the potential of MSCs to regenerate retinal neurons and delay visual impairment in retinitis pigmentosa animal models. The current study found that the GNP-labelled cells could be maintained and easily detected for one month post-injection in the subretinal layer using micro-CT. The Royal College of Surgeon rats we used belonged to a transgenic model that has defective retinal pigmented epithelium functions and could ultimately result in retinitis pigmentosa. TEM imaging revealed that the MSCs could have differentiated into retinal neuron cells when exposed to cytokines or trophic factors released by the fast-degenerating photoreceptors. In addition, we also observed possible cell differentiation into the retinal pigmented epithelium in the rats. The coupling of stem cells and nanoparticle technology may offer a relatively new and superior treatment strategy for cell replacement therapy in ocular disorders or diseases. Nanotechnology could also influence cell differentiation through intracellular particle interaction. Future studies should optimize different sizes and shapes to efficiently direct the differentiation of the GNP-loaded cells into retinal neuron cells and test for their toxicity. Lastly, we also suggest the potential use of GNP-loaded stem cells to kill cancer cells such as retinoblastoma in the eyes. Cancer cells are more sensitive to heat released by the particles when exposed to plasmonic photothermal energy. The destruction of MSCs could release important protein factors for simultaneous retinal tissue reconstruction and reparation. This paper supported the notion that nanotechnology may provide alternative research platform in stem cell tracking to new treatment modalities for cancer and regenerative medicine to improve or restore damaged tissues.

Acknowledgments: This research was supported by the Universiti Kebangsaan Malaysia-Cryocord Sdn. Bhd. Research Incentive Grant (Industri-2011-048), Ministry of Science, Technology and Innovation (MOSTI), Malaysia through the Science Fund (Grant No.: 5450817), Fundamental Research Grants Scheme (FRGS), Ministry of Education, Malaysia (Grant No.: 5524401), and the Putra Grants of Universiti Putra Malaysia, Malaysia (Grant No.: 9436300 and 9503900). The authors would like to extend their sincere appreciation to the Deanship of Scientific Research at King Saud University for funding this research group (Project No.: RG-1435-065).

Author Contributions: Pooi Ling Mok and Kong Yong Then conceived the experimental study design; Pooi Ling Mok, Sue Ngein Leow, Avin Ee-Hwan Koh, Hairul Harun Mohd Nizam, Suet Lee Shirley Ding, Shiplu Roy Chowdhury and Raduan Ruhaslizan conducted the experiments; Avin Ee-Hwan Koh and Sue Ngein Leow composed the manuscript and prepared the figures; Kong Yong Then, Suresh Kumar Subbiah, Catherine Mae-Lynn Bastion, Ruszymah Binti Hj. Idrus, Min Hwei Ng, Chi Luu, Hon Seng Wong, Akon Higuchi, Abdullah A. Alarfaj, and Wan Haslina Wan Abdul Halim supported the study design, analysed,

and commented on both data and figures; Pooi Ling Mok , Kong Yong Then, Suresh Kumar Subbiah, Akon Higuchi, and Abdullah A. Alarfaj edited the manuscript. All authors reviewed the manuscript.

Conflicts of Interest: The authors declare no conflict of interest. The funding sponsors had no role in the design of the study; in the collection, analyses, or interpretation of data; in the writing of the manuscript; and in the decision to publish the results.

References

1. Figueroa, F.E.; Carrión, F.; Villanueva, S.; Khoury, M. Mesenchymal stem cell treatment for autoimmune diseases: A critical review. *Biol. Res.* **2016**, *45*, 269–277. [CrossRef] [PubMed]
2. Karantalis, V.; Hare, J.M. Use of mesenchymal stem cells for therapy of cardiac disease. *Circ. Res.* **2015**, *116*, 1413–1430. [CrossRef] [PubMed]
3. Joyce, N.; Annett, G.; Wirthlin, L.; Olson, S.; Bauer, G.; Nolta, J. Mesenchymal stem cells for the treatment of neurodegenerative disease. *Regen. Med.* **2010**, *5*, 933–946. [CrossRef] [PubMed]
4. Kim, N.; Cho, S.G. Clinical applications of mesenchymal stem cells. *Korean J. Intern. Med.* **2013**, *28*, 387–402. [CrossRef] [PubMed]
5. Leow, S.N.; Luu, C.D.; Hairul Nizam, M.H.; Mok, P.; Ruhaslizan, R.; Wong, H.S.; Wan Abdul Halim, W.; Ng, M.H.; Ruszymah, B.; Chowdhury, S.R.; et al. Safety and efficacy of human Wharton's Jelly-derived mesenchymal stem cells therapy for retinal degeneration. *PLoS ONE* **2015**, *10*, e0128973. [CrossRef] [PubMed]
6. Bae, K.S.; Park, J.B.; Kim, H.S.; Kim, D.S.; Park, D.J.; Kang, S.J. Neuron-like differentiation of bone marrow-derived mesenchymal stem cells. *Yonsei Med. J.* **2011**, *52*, 401–412. [CrossRef] [PubMed]
7. Duscher, D.; Barrera, J.; Wong, V.W.; Maan, Z.N.; Whittam, A.J.; Januszyk, M.; Gurtner, G.C. Stem cells in wound healing: The future of regenerative medicine? A Mini-Review. *Gerontology* **2015**, *62*, 216–225. [CrossRef] [PubMed]
8. Eggenhofer, E.; Luk, F.; Dahlke, M.H.; Hoogduijn, M.J. The life and fate of mesenchymal stem cells. *Front. Immunol.* **2014**, *5*, 148. [CrossRef] [PubMed]
9. Karp, J.M.; Leng Teo, G.S. Mesenchymal stem cell homing: The devil is in the details. *Cell Stem Cell* **2009**, *4*, 206–216. [CrossRef] [PubMed]
10. Srivastava, A.K.; Bulte, J.W.M. Seeing stem cells at work in vivo. *Stem Cell Rev. Rep.* **2014**, *10*, 127–144. [CrossRef] [PubMed]
11. Bhirde, A.; Xie, J.; Swierczewska, M.; Chen, X.; Carpenter, M.K.; Frey-Vasconcells, J.; Rao, M.S.; Marin-Garcia, J.; Goldenthal, M.J.; Hart, L.S.; et al. Nanoparticles for cell labeling. *Nanoscale* **2011**, *3*, 142–153. [CrossRef] [PubMed]
12. Dreaden, E.C.; Alkilany, A.M.; Huang, X.; Murphy, C.J.; El-Sayed, M.A. The golden age: Gold nanoparticles for biomedicine. *Chem. Soc. Rev.* **2012**, *41*, 2740–2779. [CrossRef] [PubMed]
13. Ricles, L.M.; Nam, S.Y.; Treviño, E.A.; Emelianov, S.Y.; Suggs, L.J. A dual gold nanoparticle system for mesenchymal stem cell tracking. *J. Mater. Chem. B Mater. Biol. Med.* **2014**, *2*, 8220–8230. [CrossRef] [PubMed]
14. Mok, P.L.; Leong, C.F.; Cheong, S.K. Cellular mechanisms of emerging applications of mesenchymal stem cells. *Malays. J. Pathol.* **2013**, *35*, 17–32. [PubMed]
15. Ricles, L.M.; Nam, S.Y.; Sokolov, K.; Emelianov, S.Y.; Suggs, L.J. Function of mesenchymal stem cells following loading of gold nanotracers. *Int. J. Nanomed.* **2011**, *6*, 407–416. [CrossRef] [PubMed]
16. Li, J.; Li, J.J.; Zhang, J.; Wang, X.; Kawazoe, N.; Chen, G. Gold nanoparticle size and shape influence on osteogenesis of mesenchymal stem cells. *Nanoscale* **2016**, *8*, 7992–8007. [CrossRef] [PubMed]
17. Connor, E.E.; Mwamuka, J.; Gole, A.; Murphy, C.J.; Wyatt, M.D. Gold nanoparticles are taken up by human cells but do not cause acute cytotoxicity. *Small* **2005**, *1*, 325–327. [CrossRef] [PubMed]
18. Murph, S.; Jacobs, S.; Liu, J.; Hu, T.C.; Siegfired, M.; Serkiz, S.M.; Hudson, J. Manganese-gold nanoparticles as an MRI positive contrast agent in mesenchymal stem cell labeling. *J. Nanopart. Res.* **2012**, *14*, 658. [CrossRef]
19. Kohl, Y.; Gorjup, E.; Katsen-Globa, A.; Büchel, C.; von Briesen, H.; Thielecke, H. Effect of gold nanoparticles on adipogenic differentiation of human mesenchymal stem cells. *J. Nanopart. Res.* **2011**, *13*, 6789–6803. [CrossRef]
20. Choi, S.Y.; Song, M.S.; Ryu, P.D.; Lam, A.T.; Joo, S.W.; Lee, S.Y. Gold nanoparticles promote osteogenic differentiation in human adipose-derived mesenchymal stem cells through the Wnt/β-catenin signaling pathway. *Int. J. Nanomed.* **2015**, *10*, 4383–4392.

21. Kang, S.; Bhang, S.H.; Hwang, S.; Yoon, J.K.; Song, J.; Jang, H.K.; Kim, S.; Kim, B.S. Mesenchymal stem cells aggregate and deliver gold nanoparticles to tumors for photothermal therapy. *ACS Nano* **2015**, *9*, 9678–9690. [CrossRef] [PubMed]
22. D'Alessio, F.; Mirabelli, P.; Gorrese, M.; Scalia, G.; Gemei, M.; Mariotti, E.; di Noto, R.; Martinelli, P.; Fortunato, G.; Paladini, D.; et al. Polychromatic flow cytometry analysis of CD34+ hematopoietic stem cells in cryopreserved early preterm human cord blood samples. *Cytom. Part A* **2011**, *79*, 14–24. [CrossRef] [PubMed]
23. Wu, Q.; Jinde, K.; Endoh, M.; Sakai, H. Clinical significance of costimulatory molecules CD80/CD86 expression in IgA nephropathy. *Kidney Int.* **2004**, *65*, 888–896. [CrossRef] [PubMed]
24. Dominici, M.; Le Blanc, K.; Mueller, I.; Slaper-Cortenbach, I.; Marini, F.; Krause, D.; Deans, R.; Keating, A.; Prockop, D.; Horwitz, E. Minimal criteria for defining multipotent mesenchymal stromal cells. The International Society for Cellular Therapy position statement. *Cytotherapy* **2006**, *8*, 315–317. [CrossRef] [PubMed]
25. Accomasso, L.; Gallina, C.; Turinetto, V.; Giachino, C. Stem cell tracking with nanoparticles for regenerative medicine purposes: An overview. *Stem Cells Int.* **2016**, *2016*, 7920358. [CrossRef] [PubMed]
26. Meir, R.; Motiei, M.; Popovtzer, R. Gold nanoparticles for in vivo cell tracking. *Nanomedicine* **2014**, *9*, 2059–2069. [CrossRef] [PubMed]
27. Huefner, A.; Septiadi, D.; Wilts, B.D.; Patel, I.I.; Kuan, W.; Fragniere, A.; Barker, R.A.; Mahajan, S. Gold nanoparticles explore cells: Cellular uptake and their use as intracellular probes. *Methods* **2014**, *68*, 354–363. [CrossRef] [PubMed]
28. Chithrani, D. Intracellular uptake, transport, and processing of gold nanostructures. *Mol. Membr. Biol.* **2010**, *27*, 299–311. [CrossRef] [PubMed]
29. Chen, H.; Wang, L.; Yeh, J.; Wu, X.; Cao, Z.; Wang, Y.A.; Zhang, M.; Yang, L.; Mao, H. Reducing non-specific binding and uptake of nanoparticles and improving cell targeting with an antifouling PEO-b-PγMPS copolymer coating. *Biomaterials* **2010**, *31*, 5397–5407. [CrossRef] [PubMed]
30. Longmire, M.; Choyke, P.L.; Kobayashi, H. Clearance properties of nano-sized particles and molecules as imaging agents: Considerations and caveats. *Nanomedicine* **2008**, *3*, 703–717. [CrossRef] [PubMed]
31. Duan, P.; Xu, H.; Zeng, Y.; Wang, Y.; Yin, Z.Q. Human bone marrow stromal cells can differentiate to a retinal pigment epithelial phenotype when co-cultured with pig retinal pigment epithelium using a transwell system. *Cell. Physiol. Biochem.* **2013**, *31*, 601–613. [CrossRef] [PubMed]
32. Vossmerbaeumer, U.; Ohnesorge, S.; Kuehl, S.; Haapalahti, M.; Kluter, H.; Jonas, J.B.; Thierse, H.J.; Bieback, K. Retinal pigment epithelial phenotype induced in human adipose tissue-derived mesenchymal stromal cells. *Cytotherapy* **2009**, *11*, 177–188. [CrossRef] [PubMed]
33. Yang, L.; Zhou, Q.; Wang, Y.; Wang, Y.Q. Differentiation of human bone marrow-derived mesenchymal stem cells into neural-like cells by co-culture with retinal pigmented epithelial cells. *Int. J. Ophthalmol.* **2010**, *3*, 23–27. [PubMed]
34. Kevany, B.M.; Palczewski, K. Phagocytosis of retinal rod and cone photoreceptors. *Physiology* **2010**, *25*, 8–15. [CrossRef] [PubMed]
35. Guo, F.; Ding, Y.; Caberoy, N.; Alvarado, G.; Wang, F.; Chen, R.; Li, W. ABCF1 extrinsically regulates retinal pigment epithelial cell phagocytosis Running title: ABCF1 is a novel phagocytosis ligand. *Mol. Biol. Cell.* **2015**, *26*, 2311–2320. [CrossRef] [PubMed]
36. He, X.; Cai, J.; Liu, B.; Zhong, Y.; Qin, Y. Cellular magnetic resonance imaging contrast generated by the ferritin heavy chain genetic reporter under the control of a Tet-On switch. *Stem Cell Res. Ther.* **2015**, *6*, 207. [CrossRef] [PubMed]
37. Pereira, S.M.; Moss, D.; Williams, S.R.; Murray, P.; Taylor, A. Overexpression of the MRI reporter genes ferritin and transferrin receptor affect iron homeostasis and produce limited contrast in mesenchymal stem cells. *Int. J. Mol. Sci.* **2015**, *16*, 15481–15496. [CrossRef] [PubMed]
38. Amsalem, Y.; Mardor, Y.; Feinberg, M.S.; Landa, N.; Miller, L.; Daniels, D.; Ocherashvilli, A.; Holbova, R.; Yosef, O.; Barbash, I.M.; et al. Iron-oxide labeling and outcome of transplanted mesenchymal stem cells in the infarcted myocardium. *Circulation* **2007**, *116*, 138–145. [CrossRef] [PubMed]
39. Collins, M.C.; Gunst, P.R.; Cascio, W.E.; Kypson, A.P.; Muller-Borer, B.J. Labeling and imaging mesenchymal stem cells with quantum dots. *Methods Mol. Biol.* **2012**, *906*, 199–210. [PubMed]

40. Fan, J.; Li, W.; Hung, W.; Hung, W.; Chen, C.; Yeh, J. Cytotoxicity and differentiation effects of gold nanoparticles to human bone marrow mesenchymal stem cells. *Biomed. Eng. Appl. Basis Commun.* **2011**, *23*, 141–152. [CrossRef]
41. Sivan, P.P.; Syed, S.; Mok, P.L.; Higuchi, A.; Murugan, K.; Alarfaj, A.A.; Munusamy, M.A.; Hamat, R.H.; Umezawa, A.; Kumar, S. Stem Cell Therapy for Treatment of Ocular Disorders. *Stem Cells Int.* **2016**, *2016*, 8304879. [CrossRef] [PubMed]
42. Wang, M.; Li, Z.; Qiao, H.; Chen, L.; Fan, Y. Effect of Gold/Fe_3O_4 Nanoparticles on biocompatibility and neural differentiation of rat olfactory bulb neural stem cells. *J. Nanomater.* **2013**, *2013*, 867426.
43. Paviolo, C.; Haycock, J.W.; Yong, J.; Yu, A.; McArthur, S.L.; Stoddart, P.R. Plasmonic properties of gold nanoparticles can promote neuronal activity. In Proceedings of the SPIE International Society for Optics and Photonics, San Diego, CA, USA, 25–29 August 2013; Jansen, E.D., Thomas, R.J., Eds.; p. 85790C.
44. Huang, X.; El-Sayed, M.A. Gold nanoparticles: Optical properties and implementations in cancer diagnosis and photothermal therapy. *J. Adv. Res.* **2010**, *1*, 13–28. [CrossRef]
45. Kharlamov, A.; Perrish, A.; Gabinsky, J. Silica-gold nanoparticles and mesenchymal stem cells versus composite ferro-magnetic approach for management of atherosclerotic plaque and artery remodeling. *Circulation* **2011**, *124*, A8303.
46. Plasmonic Photothermal and Stem Cell Therapy of Atherosclerosis versus Stenting (NANOM PCI). Available online: https://clinicaltrials.gov/ct2/show/NCT01436123 (accessed on 30 July 2016).
47. Sarkar, D.; Vemula, P.K.; Zhao, W.; Gupta, A.; Karnik, R.; Karp, J.M. Engineered mesenchymal stem cells with self-assembled vesicles for systemic cell targeting. *Biomaterials* **2010**, *31*, 5266–5274. [CrossRef] [PubMed]
48. Khademhosseini, A.; Borenstein, J.; Toner, M.; Takayama, S. *Micro and Nanoengineering of the Cell Microenvironment*; Artech House Publishers: Norwood, MA, USA, 2008.
49. Qureshi, S. β-lactamase: An ideal reporter system for monitoring gene expression in live eukaryotic cells. *BioTechniques* **2007**, *42*, 91–95. [CrossRef] [PubMed]
50. Smale, S. Chloramphenicol acetyltransferase assay. *Cold Spring Harb. Protoc.* **2010**, *5*. [CrossRef] [PubMed]
51. Ude, C.; Shamsul, B.; Ng, M.; Chen, H.C.; Norhamdan, M.Y.; Aminuddin, B.S.; Ruszymah, B.H.I. Bone marrow and adipose stem cells can be tracked with PKH26 until post staining passage 6 in in vitro and in vivo. *Tissue Cell* **2012**, *44*, 156–163. [CrossRef] [PubMed]
52. Johnsson, C.; Festin, R.; Tufveson, G.; Tötterman, T.H. Ex vivo PKH26-labelling of lymphocytes for studies of cell migration in vivo. *Scand. J. Immunol.* **1997**, *45*, 511–514. [CrossRef] [PubMed]
53. Xu, R.; Huang, L.; Wei, W.; Chen, X.; Zhang, X.; Zhang, X. Real-time imaging and tracking of ultrastable organic dye nanoparticles in living cells. *Biomaterials* **2016**, *93*, 38–47. [CrossRef] [PubMed]
54. Martin-Fernandez, M.L.; Clarke, D.T. Single molecule fluorescence detection and tracking in mammalian cells: The state-of-the-art and future perspectives. *Int. J. Mol. Sci.* **2012**, *11*, 14742–14765. [CrossRef] [PubMed]
55. Muthana, M.; Kennerley, A.J.; Hughes, R.; Fagnano, E.; Richardson, J.; Paul, M.; Murdoch, C.; Wright, F.; Payne, C.; Lythgoe, M.F.; et al. Directing cell therapy to anatomic target sites in vivo with magnetic resonance targeting. *Nat. Commun.* **2015**, *6*, 8009. [CrossRef] [PubMed]
56. Jensen, E. Types of imaging, part 2: An overview of fluorescence microscopy. *Anat. Rec.* **2012**, *295*, 1621–1627. [CrossRef] [PubMed]
57. Progatzky, F.; Dallman, M.J.; Lo Celso, C. From seeing to believing: Labelling strategies for in vivo cell-tracking experiments. *Interface Focus* **2013**, *3*, 20130001. [CrossRef] [PubMed]
58. Edmundson, M.; Capeness, M.; Horsfall, L. Exploring the potential of metallic nanoparticles within synthetic biology. *New Biotechnol.* **2014**, *3*, 572–577. [CrossRef] [PubMed]
59. Li, J.; Kawazoe, N.; Chen, G. Gold nanoparticles with different charge and moiety induce differential cell response on mesenchymal stem cell osteogenesis. *Biomaterials* **2015**, *54*, 226–236. [CrossRef] [PubMed]